

Lead-free magnetic double perovskites for photovoltaic and photocatalysis applications

Muskan Nabi,¹ Sanika S. Padelkar,^{1,2,3,4} Jacek J. Jasieniak¹,⁴ Alexandr N. Simonov,² and Aftab Alam^{1,3,*}

¹Department of Physics, Indian Institute of Technology, Bombay, Powai, Mumbai, 400076, India

²School of Chemistry, Monash University, Victoria 3800, Australia

³IITB-Monash Research Academy, IIT Bombay, Mumbai, 400076, India

⁴Department of Materials Science and Engineering, Monash University, Victoria 3800, Australia

(Received 24 May 2023; revised 2 November 2023; accepted 18 December 2023; published 31 January 2024)

The magnetic spin degrees of freedom in magnetic materials serve as an additional way to tune materials properties, thereby invoking a magneto-optical response. Herein, we report the magneto-optoelectronic properties of a family of lead-free magnetic double perovskites of the form Cs_2AgTX_6 ($T = \text{Sc}, \text{Ti}, \text{V}, \text{Cr}, \text{Mn}, \text{Fe}, \text{Co}, \text{Ni}, \text{Cu}; X = \text{Cl}, \text{Br}, \text{I}$). These provide an extremely fertile series, giving rise to potential candidate materials for photovoltaic applications. In conjunction with a high absorption coefficient and a high simulated power-conversion efficiency for photovoltaic applications, a few compounds in this series exhibit magnetic character useful for spintronic applications. The interaction between magnetism and light can have far-reaching effects on the photovoltaic properties as a consequence of the shift in the defect energy levels due to the Zeeman effect. This subsequently affects the recombination rate of minority carriers, and hence the photoconversion efficiency. Moreover, the distinct ferromagnetic and antiferromagnetic ordering driven by hybridization and the superexchange mechanism can play a significant role in breaking the time-reversal and/or inversion symmetry. Such a coalescence of magnetism and efficient optoelectronic response has the potential to trigger a magnetic/spin anomalous photovoltaic (nonlinear optical) effect in this Cs_2AgTX_6 family. These insights can thus channelize the advancement of lead-free double perovskites in the magnetic/spin anomalous-photovoltaic-effect field as well.

DOI: 10.1103/PhysRevApplied.21.014063

I. INTRODUCTION

Organic-inorganic halide double perovskites (DPs) have emerged as a promising class of materials in various fields, such as ferroelectrics [1], spintronics [2], photovoltaics [3,4], and optoelectronic devices that include light-emitting diodes [5], sensors [6], x-ray detectors [7], and photodetectors [8]. Lead-free halide DPs with the general formula $A_2BB'X_6$, formed by the combination of one monovalent ion and one trivalent ion, have emerged ubiquitously as a stable and green alternative to toxic lead-based halide perovskites. The optoelectronic properties of these materials are associated with compositional flexibility, dielectric properties, and exciton binding energies ranging over several orders of magnitude [9,10]. Among the family of DPs, materials with $A = \text{Cs}^+$, $B = \text{Ag}^+$ or Cu^+ , and $B' = \text{Bi}^{3+}$, Sb^{3+} , or In^{3+} have been proposed to be environmentally friendly alternatives to lead-based perovskites [11]. Some of the experimentally studied materials, e.g., $\text{Cs}_2\text{AgBiX}_6$ ($X = \text{Cl}, \text{Br}, \text{I}$) [12,13], $\text{Cs}_2\text{AgSbX}_6$ [14,15], $\text{Cs}_2\text{AgInX}_6$ [16,17], and Cs_2InX_6 ($B^{3+} = \text{Sb}$,

Bi) [18,19], have received substantial interest because of their promising properties. $\text{Cs}_2\text{AgBiBr}_6$ [20] is one of the most-frequently-investigated materials in this class, having high thermodynamic stability although with an indirect band gap of about 2 eV and solar power-conversion efficiency of approximately 3%. However, recent experimental and theoretical evidence has shown that the Ag-Bi variants exhibit intrinsic and strong electronic confinement, which is manifested in very large exciton binding energies (hundreds of millielectronvolts), strong carrier localization, and reduced free-carrier mobility [21,22]. The exciton binding energies in halide DPs are influenced by the electronic structure of the alternating B -site and B' -site cations. Hence, via chemical substitution at the B and B' sites, the existing set of halide DPs can be optimized towards better performance. The seminal contributions to modulate the existing class of materials have been underpinned by several viable strategies such as alloy/doping-mediated band-gap engineering, optimizing synthesis processes with a view to tackling critical challenges [23].

However, an aspect that remains underexplored but has much promise is the magnetic spin degrees of freedom available in magnetic perovskites to tune

* aftab@iitb.ac.in

the photovoltaic (PV) properties, which in all likelihood could lead to staggering spin-related properties. In this regard, a few halide perovskites, viz., $\text{Cs}_2\text{AgT}^{3+}\text{Cl}_6$ ($T = \text{Fe}, \text{Cr}$) [24,25], $\text{Cs}_2\text{NaT}^{3+}\text{Cl}_6$ ($T = \text{Fe}, \text{V}, \text{Mn}, \text{Ni}$) [26,27], $\text{Cs}_2\text{KT}^{3+}\text{Cl}_6$ ($T = \text{Mn}, \text{Co}, \text{Ni}$) [28], and $\text{Cs}_2\text{GeT}^{3+}\text{X}_6$ ($\text{M} = \text{Ti}, \text{V}, \text{Cr}, \text{Mn}, \text{Fe}, \text{Co}, \text{Ni}, \text{Cu}$) [29], and various oxide perovskites [30,31] have been reported to show interesting magnetic properties. Among these compounds, cubic $\text{Cs}_2\text{AgFeCl}_6$ [24], in particular, has been experimentally reported to have promising optoelectronic characteristics and PV performance. Correspondingly, hexagonal $\text{Cs}_2\text{AgCrCl}_6$ [25] was synthesized in the paramagnetic phase and demonstrated significant optoelectronic properties. However, the interconnection between the magnetic degrees of freedom and the optical properties is still to be explored. The interplay of two spin degrees of freedom in these magnetic systems gives a wider platform for modulating the absorption range in an attempt to harvest the entire solar-radiation spectrum.

The oxide perovskite $\text{Bi}_2\text{FeCrO}_6$ [32] is another state-of-the-art magnetic material that has been experimentally reported to have remarkable efficiency of approximately 8%. The interaction between the magnetic field and light is called the “magneto-optical effect,” which includes the Zeeman effect, the Faraday effect, and the magneto-optical Kerr effect. The exceptional performance of $\text{Bi}_2\text{FeCrO}_6$ is attributed to two prime magneto-optical effects, viz., magnetoelectric coupling and the Zeeman effect. This system has attracted interest on account of its coexistent ferroelectric properties with inbuilt polarization—thus leading to magnetoelectric coupling. The Zeeman effect causes the energy levels to split when the material is placed in an applied magnetic field, as a consequence of which, the energy levels move from the band-gap center, reducing the recombination rate of minority carriers and thus prolonging lifetime of minority carriers. This use of magnetism to tune the optoelectronic properties is widely explored in oxide perovskites but not much has been reported for halide perovskites. The latter are good photovoltaic materials with promising photovoltaic power-conversion efficiencies [33]. So combining the magnetic effect with halide perovskites could provide opportunities for highly efficient devices.

Herein, we primarily focus on a family of halide DPs, where an amalgamation of magnetic and optoelectronic properties is discussed towards magnetophotovoltaic applications. With that perspective, we studied a set of 27 compounds of the form $\text{Cs}_2\text{AgT}^{3+}\text{X}_6$ ($T = \text{Sc}, \text{Ti}, \text{V}, \text{Cr}, \text{Mn}, \text{Fe}, \text{Co}, \text{Ni}, \text{Cu}; \text{X} = \text{Cl}, \text{Br}, \text{I}$) using *ab initio* density-functional-theory (DFT) simulation to explore the interplay between different magnetic ordering and optoelectronic properties. For example, a magnetic semiconductor with unequal band gaps in the two spin channels can capture two different ranges of the solar spectrum and hence has the capability to provide high

quantum yield. A detailed structural-and-chemical-phase-stability calculation show that 14 of the 27 compounds are in a single phase, each with different magnetic ordering. A few others also show robust stability but with the possibility of the formation of a secondary phase. Because of the presence of 3d transition elements (T^{3+}), this family of compounds provides fertile ground to realize several interesting properties, such as half-metallic ferromagnets, antiferromagnetic (AFM) semiconductors, and ferromagnetic (FM) and nonmagnetic (NM) semiconductors. On the basis of these versatile properties, these compounds are classified for different renewable-energy applications. Such a detailed study of synthesizability, electronic and magnetic structure, and optoelectronic properties provides a guiding path for experimentalists for future exploration of these magnetic perovskites.

II. COMPUTATIONAL DETAILS

All calculations were performed with DFT as implemented in Vienna Ab initio Simulation Package [34, 35]. For spin-polarized calculations, the Perdew-Burke-Ernzerhof electronic exchange-correlation functional [36] was used within the generalized-gradient approximation [37] along with projected-augmented-wave pseudopotentials [38,39]. For the wave-function expansion, a plane-wave energy cutoff of 350 eV was used for all calculations. The Brillouin-zone integration was done with the tetrahedron method with use of an $8 \times 8 \times 8$ \mathbf{k} -point grid for structural optimization, while for self-consistent-field calculations, a Γ -centered \mathbf{k} -point mesh of size $12 \times 12 \times 12$ was used. Keeping in mind the possibility of both cubic and hexagonal phases (as experimentally reported for two different systems belonging to this class) along with different magnetic ordering, we performed structural optimization for all the compounds in both these phases considering NM, FM, and AFM ordering. The force (energy) was converged up to 10^{-3} eV Å⁻¹ (10^{-6} eV).

Because of the strongly correlated nature of the 3d transition elements, an “on-site” Hubbard potential (U) [40] was applied to capture the intra-atomic interactions between these strongly correlated electrons. U was calculated with the linear-response ansatz of Cococcioni *et al.* [41]. The calculation procedure and the simulated U values for different systems are presented in Sec. S1 (see Fig. S1 and Table S1) of Supplemental Material [42]; also see Refs. [43–51]. To estimate the theoretical photoconversion efficiency, we report the spectroscopic limited maximum efficiency (SLME) of the semiconducting systems [52].

III. RESULTS AND DISCUSSION

A. Structural and chemical phase stability

The structural stability of the halide DPs [53] is dictated by a geometrical tolerance factor (t) defined as

$$t = \frac{r_A + r_X}{\sqrt{2(r_{av} + r_X)}}, \quad (1)$$

where r_A , r_X , and r_{av} are the Shannon ionic radii of A cations and X anions and the average ionic radius of B and B' cations, respectively. Table S2 in Supplemental Material [42] shows the tolerance factor of all the compounds that are found to lie in the t range from 0.91 to 0.98, predicting these compounds will stabilize in the cubic structure. Interestingly, $\text{Cs}_2\text{AgCrCl}_6$ [25] was experimentally reported to crystallize in the hexagonal phase, which is normally associated with values of t greater than 1. Certainly, there are other instances where the ideal cubic structure is not observed experimentally, departing from these purely geometrical tolerance-factor guidelines [54,55]. There are also other factors, such as B cation off-centering and the presence and stereoactivity of a lone pair of electrons, that are also suggested to have a strong impact on the geometrical stability of perovskites in general [56–58]. However, for transition metal-based perovskites, the nonbonding (lone) pairs of electrons in transition metals do not influence the molecular geometry and are said to be stereochemically inactive. Hence, we believe that the presence of lone pairs in transition metals will not affect the molecular geometry of the BX_6 octahedra in $A_2BB'X_6$ DPs. To address the above-mentioned ambiguities, we investigated the chemical and thermodynamic stability in both the cubic phase and the hexagonal phase for the entire series.

For the cubic structure of Cs_2AgTX_6 , a 40-atom conventional unit cell [space group $Fm\bar{3}m$ (no. 225)] was considered, in which Cs is enclosed by a cage of 12 X atoms, while Ag and T form corner-sharing AgX_6 and TX_6 octahedra, as shown in Fig. 1(a). The Wyckoff positions of

Cs, Ag, T and X were 8c (0.25, 0.25, 0.25), 4b (0.5, 0.5, 0.5), 4a (0, 0, 0), and 24e (0.24, 0, 0), respectively. For the hexagonal phase, we used a 20-atom primitive unit cell [space group $R\bar{3}m$ (no. 166)] adopting a $\text{Ba}_2\text{NiTeO}_6$ -type structure [59]; see Fig. 1(b). The Wyckoff positions in this case were 6c (0, 0, 0.21), 6c (0, 0, 0.37), 3a (0, 0, 0), and 8h (0.48, \bar{x} , 0.24) for Cs, Ag, T , and X , respectively. To assess the thermodynamic stability, we calculated the formation energy (ΔE_F) of all the compounds in both the cubic phase and the hexagonal phase considering three different magnetic orderings (NM, FM, and AFM), as depicted in Fig. 2, where an asterisk indicates the energetically stable phase for a given compound.

Negative ΔE_F indicate the thermodynamic possibility of the formation of these compound. Herein, a comparison of the data for materials with different halides suggests that chloride-based compounds are more robust than those based on bromide and iodide. This trend validates the available experimental findings, according to which bromide-based and chloride-based halide DPs are easier to synthesize than their iodide counterparts. Unsurprisingly, experimental reports on the latter are quite rare [60]. The actual formation energies of all the examined compounds in their respective stable structural or magnetic phase are provided in Table S3 in Supplemental Material [42].

Experimentally, $\text{Cs}_2\text{AgFeCl}_6$ [24,61] and $\text{Cs}_2\text{AgCrCl}_6$ [25] are reported to crystallize in cubic (with antiferromagnetic nature at low temperature) and hexagonal structures, respectively. Because of the involvement of 3d transition elements (Fe and Cr), these compounds are expected to show rich magnetic phase diagrams, including the possibility of distinct magnetic ordering such as FM or AFM in the lower-temperature range. This aspect of the

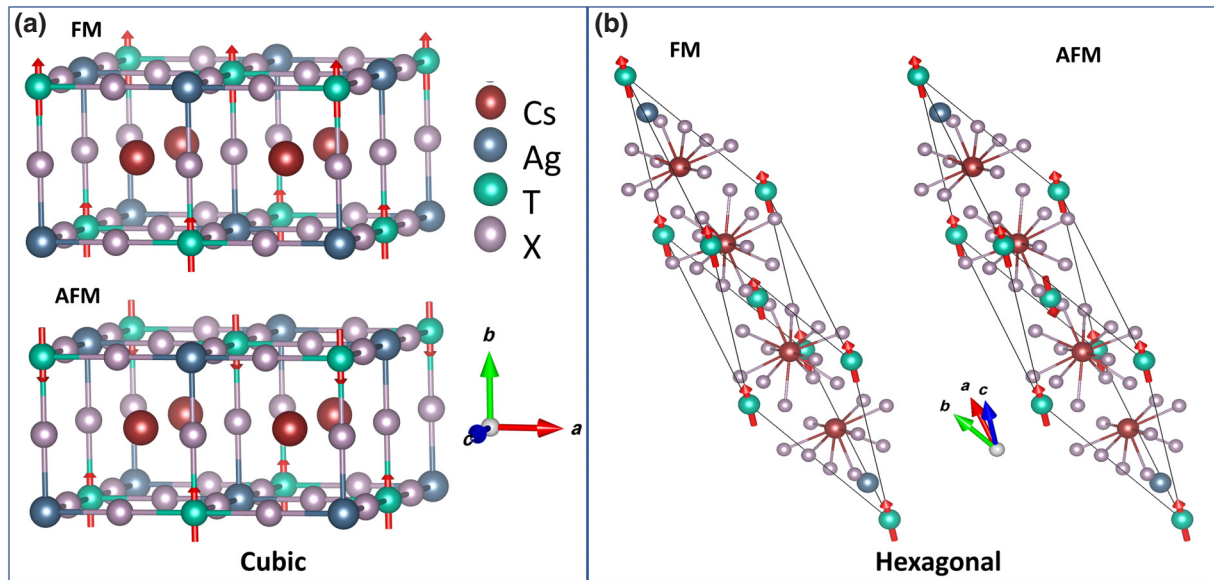


FIG. 1. Crystal structure of Cs_2AgTX_6 (where T is a transition element) in (a) the cubic and (b) hexagonal phases. FM and AFM indicate ferromagnetic and antiferromagnetic ordering, respectively.

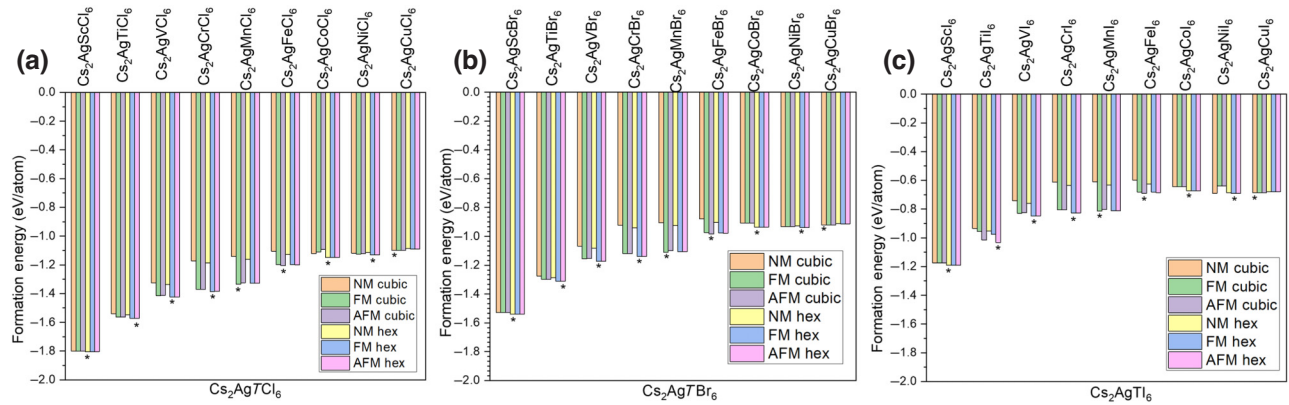


FIG. 2. Formation energies (ΔE_F) of Cs_2AgTX_6 ($T = \text{Sc}, \text{Ti}, \text{V}, \text{Cr}, \text{Mn}, \text{Fe}, \text{Co}, \text{Ni}, \text{Cu}; X = \text{Cl}, \text{Br}, \text{I}$) in two different structures [cubic and hexagonal (hex)] and three different magnetic phases (NM, FM, and AFM). An asterisk indicates the energetically stable phase for each compound.

aforementioned systems is overlooked in the literature but it can be extremely important to dictate their overall magneto-optical properties. Therefore, we studied all the compounds in different magnetic configurations—namely, NM, FM, and AFM.

Remarkably, the magnetic as well as the structural phases of these compounds are not significantly affected by the chemical nature of the halide anion, indicating that perhaps the transition element T^{3+} plays a pivotal role in determining the crystal/magnetic structure of these systems. However, the tolerance factor raises uncertainty in the experimentally stable structural phase, as observed in the case of $\text{Cs}_2\text{AgCrCl}_6$ [25]. Apparently, the simulated thermodynamic chemical phase diagram gives more-accurate information about the degree of synthesizability

of such compounds (i.e., whether in the cubic or hexagonal phase and/or the NM, FM, or AFM phase). The chemical phase diagrams of the experimentally synthesized systems $\text{Cs}_2\text{AgFeCl}_6$ [24] and $\text{Cs}_2\text{AgCrCl}_6$ [25] are shown in Fig. 3. They display a narrow stable region (shown by the gray area) in comparison with the competing secondary phases. For each of these two compounds, ten secondary phases were simulated to draw their phase diagrams (see Table S4 in Supplemental Material [42]). The narrow stable region indicates that it may be an arduous task to synthesize these systems in a single phase. From analysis of the energetics in our calculations, the most-competing secondary phases for the two systems are $\text{Cs}_3\text{Fe}_2\text{Cl}_9$ and $\text{Cs}_3\text{Cr}_2\text{Cl}_9$, which, depending on the synthesis conditions, may restrain the respective target phases

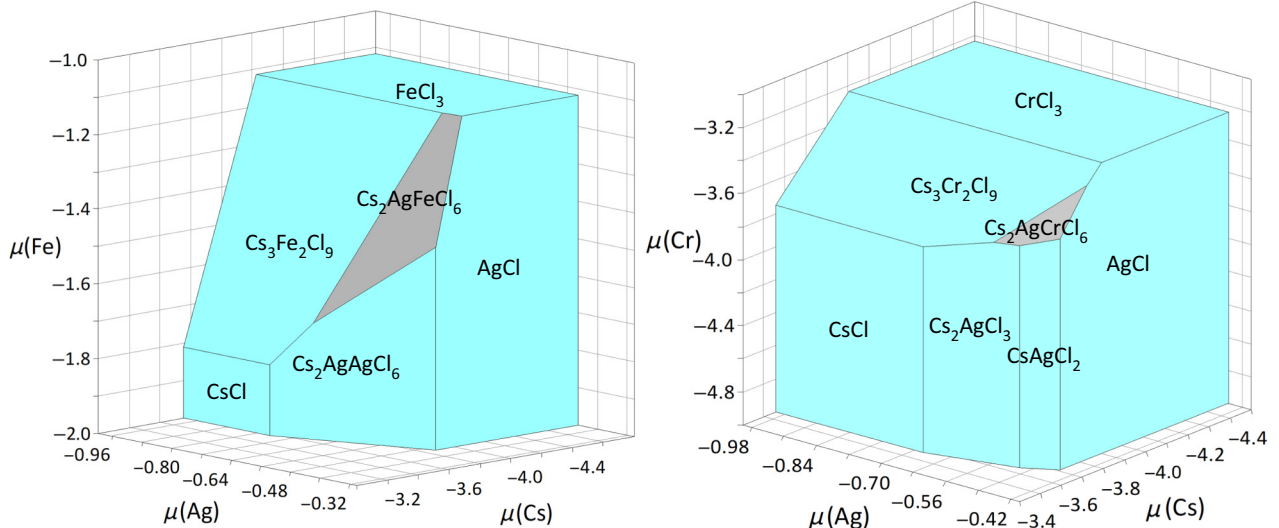


FIG. 3. Chemical phase diagrams of (a) $\text{Cs}_2\text{AgFeCl}_6$ and (b) $\text{Cs}_2\text{AgCrCl}_6$. The gray area indicates the extent of the stability region for the target systems, whereas the cyan area represents secondary phases.

$\text{Cs}_2\text{AgFeCl}_6$ and $\text{Cs}_2\text{AgCrCl}_6$ to remain stable in a single phase. There is a possibility of the coexistence of binary phases in the synthesized compounds, with a slight dominance of $\text{Cs}_3\text{Fe}_2\text{Cl}_9$ over $\text{Cs}_2\text{AgFeCl}_6$. Recently, the phase segregation and existence of secondary phases along with the target phase have also been observed in Cs-Pb-Br thin films [62]. For example, Caicedo-Dávila *et al.* [63] reported the coexistence of CsPbBr_5 and CsPbBr_3 during the synthesis of CsPbBr_5 on the basis of competing-phase-diagram analysis, which was further validated by the DFT calculations. Also, Yu *et al.* [64] confirmed that the coexistence of CsPb_2Br_5 and CsPbBr_3 is inevitable during the synthesis of CsPb_2Br_5 .

However, the presence of binary phases can be negated by optimization of the synthesis process and variation of the environmental parameters, such as pressure. There are reports where pressure is used as an important parameter to study the structural-property relationships [65]. To cross-check the pressure effect, we performed DFT calculations for two compounds, $\text{Cs}_2\text{AgFeCl}_6$ and $\text{Cs}_2\text{AgCrCl}_6$, by systematically varying the lattice constant, which in turn results in a change in the unit-cell volume and hence the pressure. In the case of $\text{Cs}_2\text{AgFeCl}_6$ and $\text{Cs}_2\text{AgCrCl}_6$, we studied the chemical stability over a range of pressure from 0 to 44 kbar and from 0 to 18.82 kbar respectively. The chemical phase stability diagrams of these compounds in the above-mentioned pressure ranges are presented in Fig. S3 in Supplemental Material [42]. It can be observed that the stability region of the target phase decreases. Although the synthesizability of $\text{Cs}_2\text{AgFeCl}_6$ and $\text{Cs}_2\text{AgCrCl}_6$ decreases with increase in pressure, it is important to note that both $\text{Cs}_2\text{AgFeCl}_6$ and $\text{Cs}_2\text{AgCrCl}_6$ have been synthesized experimentally in ambient conditions. So, from the chemical stability point of view, we confirm that $\text{Cs}_2\text{AgFeCl}_6$ [61] crystallizes in a cubic structure with AFM ordering, while $\text{Cs}_2\text{AgCrCl}_6$ crystallizes in a hexagonal structure with ferromagnetic ordering. We simulated the chemical phase diagrams of the rest of the compounds in the series as well, and found 14 of the 27 compounds stabilize in a single phase (see Fig. S2 in Supplemental Material [42]). The respective competing secondary phases used for each target compound are provided in Table S4 in Supplemental Material [42]. These 14 compounds are $\text{Cs}_2\text{AgScI}_6$, $\text{Cs}_2\text{AgScBr}_6$, $\text{Cs}_2\text{AgScCl}_6$, $\text{Cs}_2\text{AgVBr}_6$, $\text{Cs}_2\text{AgVCl}_6$, $\text{Cs}_2\text{AgCrBr}_6$, $\text{Cs}_2\text{AgCrCl}_6$, $\text{Cs}_2\text{AgMnBr}_6$, $\text{Cs}_2\text{AgMnCl}_6$, $\text{Cs}_2\text{AgFeBr}_6$, $\text{Cs}_2\text{AgFeCl}_6$, $\text{Cs}_2\text{AgCoBr}_6$, $\text{Cs}_2\text{AgCoCl}_6$, and $\text{Cs}_2\text{AgNiCl}_6$. Of these 14 compounds, only the iodide-based perovskite ($\text{Cs}_2\text{AgScI}_6$) is predicted to be stable, again confirming the difficulty in stabilizing the DPs with this anion.

Interestingly, comparison of the chemical phase stability diagram (Fig. S4) indicates a larger stability region for Cs_2AgTX_6 ($T = \text{Fe}, \text{Cl}$) as compared with $\text{Cs}_2\text{AgBiBr}_6$, confirming the ease of synthesis and relative robustness of

the former. Along similar lines, it was previously reported that the influence of structural dynamics in the halide double perovskite $\text{Cs}_2\text{AgBiBr}_6$ is weaker than that in halide single perovskites [66]. To assess and compare the influence of structural dynamics on this class of magnetic halide DPs, we performed phonon-dispersion calculations for $\text{Cs}_2\text{AgFeCl}_6$. In Fig. S4(d), we compare the dynamical stability of $\text{Cs}_2\text{AgFeCl}_6$ with that of $\text{Cs}_2\text{AgBiBr}_6$ and CsPbBr_3 at 0 K. One can notice the appearance of relatively higher imaginary frequencies in the case of $\text{Cs}_2\text{AgBiBr}_6$ [67] and CsPbBr_3 [68] due to the highly anharmonic nature of the force constants as compared with $\text{Cs}_2\text{AgFeCl}_6$, confirming the greater stability of the latter. The above comparison support the smaller influence of structural dynamics in our reported magnetic halide DPs as compared with $\text{Cs}_2\text{AgBiBr}_6$ and CsPbBr_3 .

B. Electronic structure and magnetic properties

Table I shows the band gap (E_g), the difference between the direct band gap and the indirect band gap (Δ), and atom-projected magnetic moments on the transition elements (T) for all 14 stable compounds, as mentioned in the previous section. Similar details for all 27 compounds (Cs_2AgTX_6) are presented in Table S5 in Supplemental Material [42]. Most energetically stable structure and

TABLE I. Magnitude and nature of the band gap (E_g), difference between the direct band gap and the indirect band gap (Δ), and local magnetic moment on T atoms (m_T) of 14 chemically stable Cs_2AgTX_6 compounds. \uparrow and \downarrow stand for the spin-up and spin-down channels respectively. The description within parentheses for every system indicates the stable phase.

Cs_2AgTX_6	E_g (eV)	Δ (eV)	m_T (μ_B)
$\text{Cs}_2\text{AgScCl}_6$ (hexagonal NM)	3.64 (indirect)	0.01	...
$\text{Cs}_2\text{AgVCl}_6$ (hexagonal FM)	(\uparrow) 2.40 (indirect)	0.01	1.93
	(\downarrow) 2.46 (indirect)	0.07	
$\text{Cs}_2\text{AgCrCl}_6$ (hexagonal FM)	(\uparrow) 1.69 (indirect)	0.02	3.15
	(\downarrow) 3.51 (indirect)	0.07	
$\text{Cs}_2\text{AgMnCl}_6$ (cubic FM)	(\uparrow) metallic	...	4.3
	(\downarrow) 3.81 (direct)	...	
$\text{Cs}_2\text{AgFeCl}_6$ (cubic AFM)	1.17 (direct)	...	4.12
$\text{Cs}_2\text{AgCoCl}_6$ (hexagonal NM)	1.27 (indirect)	0.03	...
$\text{Cs}_2\text{AgScBr}_6$ (hexagonal NM)	2.89 (indirect)	0.03	...
$\text{Cs}_2\text{AgVBr}_6$ (hexagonal FM)	(\uparrow) 1.95 (indirect)	0.13	1.99
	(\downarrow) 3.00 (indirect)	0.11	
$\text{Cs}_2\text{AgCrBr}_6$ (hexagonal FM)	(\uparrow) 1.09 (indirect)	0.05	3.33
	(\downarrow) 3.19 (indirect)	0.09	
$\text{Cs}_2\text{AgMnBr}_6$ (cubic FM)	(\uparrow) metallic	...	4.32
	(\downarrow) 2.87 (direct)	...	
$\text{Cs}_2\text{AgFeBr}_6$ (cubic AFM)	0.64 (direct)	...	3.98
$\text{Cs}_2\text{AgCoBr}_6$ (hexagonal NM)	0.96 (indirect)	0.05	...
$\text{Cs}_2\text{AgNiBr}_6$ (hexagonal FM)	(\uparrow) metallic	...	1.66
	(\downarrow) 1.93 (direct)	0.03	
$\text{Cs}_2\text{AgScI}_6$ (hexagonal NM)	2.51 (indirect)	0.08	...

the corresponding magnetic phase for each compound are given in parentheses in the first columns of Table 1 and S5. To correctly capture the effect of electron-electron correlation arising from transition elements, we applied an on-site Hubbard U correction for each compound, which was calculated self-consistently. On inclusion of the Hubbard potential, the degeneracy of d states found around the Fermi level is lifted in some of the compounds examined, resulting in an increase of the band gap. As follows from the data in Table I, this set of compounds shows diverse electronic and magnetic properties ranging from nonmagnetic metals and semiconductors to ferromagnetic half-metals to antiferromagnetic semiconductors and ferromagnetic semiconductors.

Compounds of the form $\text{Cs}_2\text{AgFe}X_6$ ($X = \text{Cl}, \text{Br}, \text{I}$) have a direct band gap (E_g), with E_g values ranging from 1.17 eV (Cl) to 0.64 eV (Br) to 0.12 eV (I). Although the other compounds have an indirect band gap, the difference (Δ) between the direct band gap and the indirect band gap is quite small (ranging from 0.01 to 0.09 eV). As expected, the band gap decreases owing to the decrease in the electronegativity of the halogens, as observed in other halide perovskites as well [69]. The magnetism in some of these compounds arises mainly from the partially filled transition d elements at the T site (Table I). Hence, the presence of unpaired electrons in the d orbitals of transition elements, mainly contributes to the magnetic behavior of the compound in Cs_2AgTX_6 series. On the basis of these electronic and magnetic properties, one can classify these materials into compounds with (1) moderate band gaps, (2) large band gaps, and (3) metallic nature in one spin channel and semiconducting nature in the other (half-metals). Such varied properties can make these materials useful for applications such as photovoltaics, photo(electro)catalysis, and spintronics, which needs further in-depth analysis (see Sec. 3 of Supplemental Material [42] for more details).

To explore the potential of these materials for magnetophotovoltaic application, two experimentally synthesized compounds, $\text{Cs}_2\text{AgFeCl}_6$ [24] and $\text{Cs}_2\text{AgCrCl}_6$ [25], that show two distinct magnetic orderings (AFM and FM, respectively) were chosen for deeper examination. Figures 4(a) and 4(b) show the bulk electronic band structures of these two materials. The magnetic ordering preferably shows up at low temperature, which to the best of our knowledge has not been experimentally observed. Our simulation show $\text{Cs}_2\text{AgFeCl}_6$ to be antiferromagnetic with a band gap of around 1.17 eV, which agrees fairly well with the experimental value of 1.55 eV [24]. The valence-band maximum (VBM) and the conduction-band minimum (CBM) lie at a common high-symmetry X point, resulting in a direct band gap. From the partial density of states (PDOS), one can see that the CBM is composed mostly of the Fe d states hybridized with some of the Cl p states, with a slight contribution from the Ag d states. The VBM is composed mostly of the Cl p and

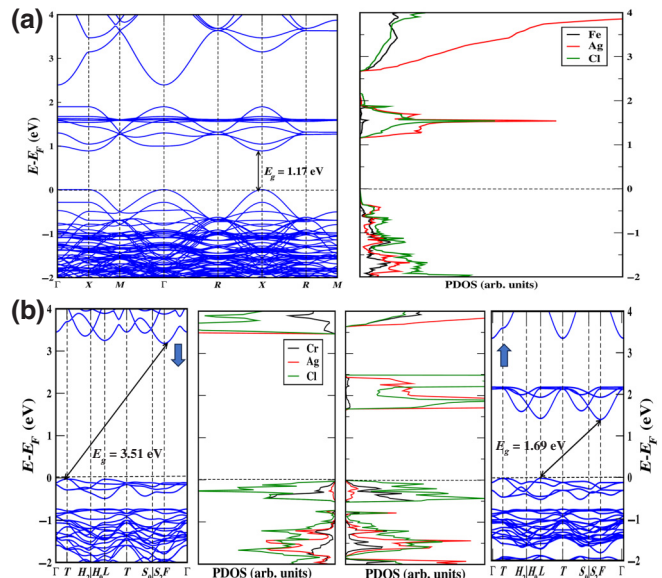


FIG. 4. Spin-resolved band structure and PDOS for (a) cubic AFM $\text{Cs}_2\text{AgFeCl}_6$ and (b) hexagonal FM $\text{Cs}_2\text{AgCrCl}_6$. The former is an AFM semiconductor with a band gap of 1.17 eV, while the latter is a FM semiconductor with band gaps of 3.51 and 1.69 eV for spin-down and spin-up channels, respectively.

Ag d states. The strong hybridization between these states near the VBM is responsible for strong band dispersion, leading to low effective mass of holes and hence higher mobility of holes as compared with electrons, indicating the p -type semiconducting behavior of $\text{Cs}_2\text{AgFeCl}_6$. Using the semiclassical Boltzmann transport theory within the constant-relaxation-time approximation [70], we simulated the carrier mobilities of $\text{Cs}_2\text{AgFeCl}_6$ and $\text{Cs}_2\text{AgCrCl}_6$. These are essentially the free-carrier mobility and hence set an upper bound on this quantity. Figure S9 in Supplemental Material [42] shows a comparative plot of electron and hole mobilities of $\text{Cs}_2\text{AgFeCl}_6$ and $\text{Cs}_2\text{AgCrCl}_6$ across the temperature range at a carrier concentration of 10^{10} cm^{-3} . For comparison, carrier mobilities for $\text{Cs}_2\text{AgBiBr}_6$, a well-studied DP, are also shown. The Cs s states are scant around the Fermi level and dominantly lie deep down the conduction band and hence play a passive role in defining the electronic properties. Because of the AFM ordering, the net magnetization of the unit cell is zero, while the atom-projected Fe moment is approximately $4.12\mu_B$. In case of $\text{Cs}_2\text{AgFeCl}_6$ and its counter bromine and iodine analogues ($\text{Cs}_2\text{AgFeBr}_6$ and $\text{Cs}_2\text{AgFeI}_6$) the orbital contribution to density of states is same as $\text{Cs}_2\text{AgFeCl}_6$ only the value of band gap decreases as expected.

Next we consider $\text{Cs}_2\text{AgCrCl}_6$, which is a ferromagnetic semiconductor [Fig. 4(b)]. It has two different semiconducting band gaps (E_g) in two spin channels. In the spin-down channel, the CBM lies at the high-symmetry F point, while the VBM lies at the T point, producing an

indirect band gap ($E_g = 3.15$ eV). In the spin-up channel, the CBM also lies at the F point, but the VBM occur at the L point, with an indirect band gap of 1.69 eV. From the PDOS plot, one can notice a hybridization between the Cl p and Ag d states in the valence band in both spin channels. In the spin-up channel, the conduction band is composed mostly of the Cr d states, with some contribution from the p states. In both spin channels, the Ag d states reside near the valence band because it has full d valence electrons. The d orbitals of Cr are half filled with three unpaired electrons, giving rise to a net moment of approximately $3.1\mu_B$. The electronic band structure and the DOS for the rest of the chemically stable compounds (Cs_2AgTX_6) are given in Figs. S5–S8 in Supplemental Material [42]. Robust chemical stability, optimal band gap, and varying magnetic orderings make these materials potential candidates for magnetophotovoltaic applications.

C. Optical properties

Hybrid halide perovskites have proven to be potential candidates for photovoltaic applications owing to factors such as high absorption coefficients and suitable band gaps. The equation relating the optical absorption coefficient (α) to the dielectric function (ϵ) is:

$$\alpha(\omega) = \sqrt{2\omega/c} * [\sqrt{\text{Re}(\epsilon_1(\omega^2)) + \text{Im}(\epsilon_2(\omega^2))} - \text{Re}(\epsilon_1(\omega^{-2}))] \quad (2)$$

where c is the speed of light, ϵ_1 and ϵ_2 represent the real and imaginary parts of the dielectric function, and ω is the frequency. ϵ_2 was calculated by use of the independent-particle approximation [71] and ϵ_1 was calculated from the DFT-simulated ϵ_2 with use of the Kramers-Kronig relation [72]. In the case of the hexagonal structure, the dielectric tensor is diagonal with two different components: $\epsilon_{2\alpha_{zz}}$ (along the z axis of the crystal), and $\epsilon_{2\alpha_{xx}}$ and $\epsilon_{2\alpha_{yy}}$ (along any direction in the plane perpendicular to the hexagonal z axis). On the basis of the optimal band-gap values in the visible range, a few of the compounds, viz., $\text{Cs}_2\text{AgCoI}_6$, $\text{Cs}_2\text{AgCoBr}_6$, $\text{Cs}_2\text{AgCoCl}_6$, $\text{Cs}_2\text{AgFeBr}_6$, $\text{Cs}_2\text{AgFeCl}_6$, $\text{Cs}_2\text{AgCrI}_6$, $\text{Cs}_2\text{AgCrBr}_6$, $\text{Cs}_2\text{AgCrCl}_6$, and $\text{Cs}_2\text{AgVBr}_6$, were found to be promising for PV applications. The optical absorption of most of these compounds is relatively high (more than $3 \times 10^5 \text{ cm}^{-1}$), as shown in Figs. 5(a)–5(f). The onset of the absorption curves corresponds to the respective band gaps (Table I). For example, in the case of $\text{Cs}_2\text{AgFeCl}_6$, one can observe that onset of optical absorption is at around 1.17 eV, which matches our simulated electronic band gap.

To quantify the power-conversion efficiency, the SLME, as introduced by Yu *et al.* [52], was estimated (see Sec. 3.1 of Supplemental Material [42] for more details). For the SLME, the input parameters are the band gap, the absorption coefficient, the standard solar spectrum,

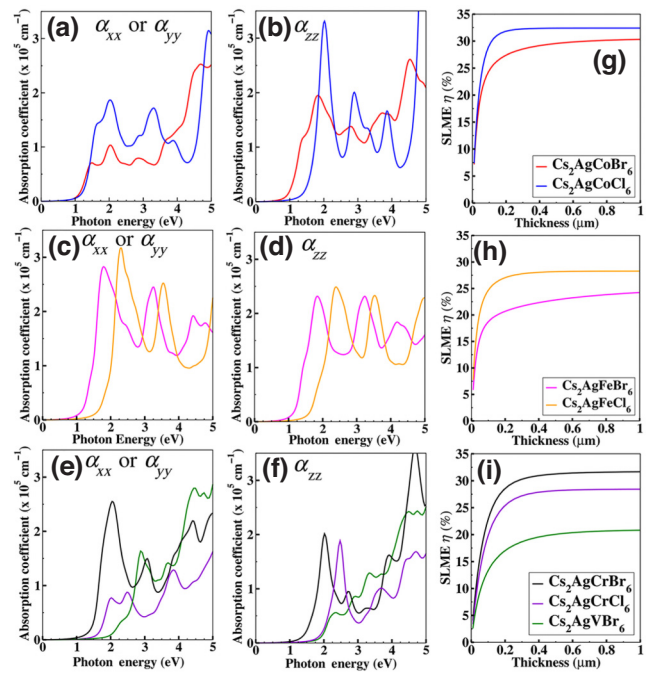


FIG. 5. Absorption coefficient (α_{ii}) in the in-plane direction and the out-of-plane direction for selected (a),(b) nonmagnetic, (c),(d) antiferromagnetic, and (e),(f) ferromagnetic systems. SLME of the same set of (g) nonmagnetic, (h) antiferromagnetic, and (i) ferromagnetic systems.

and the thickness. Figures 5(g)–5(i) show the simulated SLME for all the compounds shortlisted for PV application. The calculated SLME for an absorber-layer thickness of 1 μm is 23.09%, 30.57%, 32.41%, 25.52%, 28.82%, 17.42%, 31.72%, 28.45%, and 20.93%, for $\text{Cs}_2\text{AgCoI}_6$, $\text{Cs}_2\text{AgCoBr}_6$, $\text{Cs}_2\text{AgCoCl}_6$, $\text{Cs}_2\text{AgFeBr}_6$, $\text{Cs}_2\text{AgFeCl}_6$, $\text{Cs}_2\text{AgCrI}_6$, $\text{Cs}_2\text{AgCrBr}_6$, $\text{Cs}_2\text{AgCrCl}_6$, and $\text{Cs}_2\text{AgVBr}_6$, respectively. Interestingly, all these materials have high SLME values even for a smaller absorber-layer thickness. This, along with their suitable band gap and high absorption coefficient, makes them potential candidates for thin-film solar cells. The highest SLME is achieved with $\text{Cs}_2\text{AgCoCl}_6$, which could serve as the best material for PV applications. $\text{Cs}_2\text{AgCrBr}_6$, which is a ferromagnetic semiconductor, exhibits a high absorption coefficients and high SLME (approximately 31%), and hence could be a promising candidate for magnetophotovoltaic applications. It is, however, important to mention that excitonic effects cannot be fully accounted for in our absorption-coefficient calculations. The method rather incorporates some weak Coulomb screening. Although this by no means reduces the impact of our findings from an overall perspective, it is a constraint on the SLME model used here. Yet another interesting candidate is $\text{Cs}_2\text{AgFeCl}_6$, which shows highly dispersive bands around the high-symmetry X point [Fig. 4(a)], implying a low effective mass of hole

charge carriers and high hole mobility as mentioned earlier. Both the VBM and the CBM are dominated by $T\ d$ states located at the X point, giving rise to a direct band gap. In contrast, for $\text{Cs}_2\text{AgCrCl}_6$, two peaks are observed in the optical absorption spectrum, which corresponds to two different band gaps in the two spin channels. These two peaks can be assigned to the $d-d$ transitions at 3.51 and 1.69 eV, respectively. With varying halides (Cl to Br to I), there is a significant shift in the onset of optical absorption, indicating a change in the electronic band gaps.

IV. CONCLUSION

The interplay of magnetic and optical properties can lead to a new avenue for finding candidate materials with promising PV performance. The purpose of this work was to explore the said objective in a family of lead-free magnetic DPs of the form $\text{Cs}_2\text{Ag}TX_6$ (where $T = \text{Sc}, \text{Ti}, \text{V}, \text{Cr}, \text{Mn}, \text{Fe}, \text{Co}, \text{Ni}, \text{Cu}; X = \text{Cl}, \text{Br}, \text{I}$). The combination of two transition elements (Ag and T) offers a wide range of intriguing magneto-optoelectronic properties. From 27 compounds, seven prospective compounds— $\text{Cs}_2\text{AgCoBr}_6$, $\text{Cs}_2\text{AgCoCl}_6$, $\text{Cs}_2\text{AgFeBr}_6$, $\text{Cs}_2\text{AgFeCl}_6$, $\text{Cs}_2\text{AgCrBr}_6$, $\text{Cs}_2\text{AgCrCl}_6$, and $\text{Cs}_2\text{AgVBr}_6$ —showed visible-light-driven band gaps, good absorption coefficients, and high power-conversion efficiency, substantiating their potential as potential PV absorbers. The rest of the compounds in the series have the potential to show significant promise in the field of photo(electro)catalysis and spintronics, on the basis of their electronic properties. The driving mechanism for the distinct magnetic properties in these compounds is hybridization and superexchange. Among the magnetic compounds in this series, $\text{Cs}_2\text{AgCrI}_6$, $\text{Cs}_2\text{AgCrBr}_6$, $\text{Cs}_2\text{AgCrCl}_6$, and $\text{Cs}_2\text{AgVBr}_6$ stabilize in hexagonal symmetry with ferromagnetic or antiferromagnetic ordering. This can incite broken time-reversal or inversion symmetry and lead to a bulk spin photovoltaic effect, thereby enhancing the PV performance due to nonlinear optical effects. For instance, large photoconductivity has been reported in CrI_3 due to the magnetism-mediated asymmetry in its antiferromagnetic ordered structure [73]. Such asymmetry has paved a unique way to explore the novel properties of magnetic materials for the anomalous photovoltaic effect. Hence, the insights into magnetic DPs of the form $\text{Cs}_2\text{Ag}TX_6$ reported in this work can channelize the advancement of perovskites in the field of the magnetic/spin anomalous photovoltaic effect. The theoretical reaffirmation of the synthesizability of our proposed compounds paves the way to also expedite experimental research in the $\text{Cs}_2\text{Ag}TX_6$ family.

ACKNOWLEDGMENTS

A.A acknowledges use of the computing facility (spacetime2) provided by IIT Bombay to support this

research. A.N.S. acknowledges Australian Research Council Future Fellowship No. FT200100317. J.J. acknowledges financially the Australian Research Council-funded Centre of Excellence in Exciton Science (Grant No. CE170100026). S.S.P. acknowledge computational support by the MASSIVE high-performance computing facility and the Monash eResearch Centre and eSolutions-Research Support Services through the use of the MonARCH high-performance-computing cluster.

M.N. and S.S.P. contributed equally to this work.

-
- [1] Xitao Liu, Zhiyun Xu, Peiqing Long, Yunpeng Yao, Chengmin Ji, Lina Li, Zhihua Sun, Maochun Hong, and Junhua Luo, A multiaxial layered halide double perovskite ferroelectric with multiple ferroic orders, *Chem. Mater.* **32**, 8965 (2020).
 - [2] Weihua Ning, Jinke Bao, Yuttapoom Puttisong, Fabrizio Moro, Libor Kobera, Seiya Shimono, Linqin Wang, Fuxiang Ji, Maria Cuartero, Shogo Kawaguchi, *et al.*, Magnetizing lead-free halide double perovskites, *Sci. Adv.* **6**, eabb5381 (2020).
 - [3] Kang Wang, Zhiwen Jin, Lei Liang, Hui Bian, Dongliang Bai, Haoran Wang, Jingru Zhang, Qian Wang, and Shengzhong Liu, All-inorganic cesium lead iodide perovskite solar cells with stabilized efficiency beyond 15%, *Nat. Commun.* **9**, 4544 (2018).
 - [4] George Volonakis, Amir Abbas Haghimirad, Rebecca L. Milot, Weng H. Sio, Marina R. Filip, Bernard Wenger, Michael B. Johnston, Laura M. Herz, Henry J. Snaith, and Feliciano Giustino, $\text{Cs}_2\text{InAgCl}_6$: a new lead-free halide double perovskite with direct band gap, *J. Phys. Chem. Lett.* **8**, 772 (2017).
 - [5] Huidong Tang, Yanqiao Xu, Xiaobo Hu, Qing Hu, Ting Chen, Weihui Jiang, Lianjun Wang, and Wan Jiang, Lead-free halide double perovskite nanocrystals for light-emitting applications: Strategies for boosting efficiency and stability, *Adv. Sci.* **8**, 2004118 (2021).
 - [6] Zhihui Rao, Qiaoqiao Li, Zhilin Li, Liujiang Zhou, Xiujian Zhao, and Xiao Gong, Ultra-high-sensitive temperature sensing based on Er^{3+} and Yb^{3+} Co-doped lead-free double perovskite microcrystals, *J. Phys. Chem. Lett.* **13**, 3623 (2022).
 - [7] Yuki Haruta, Mioko Kawakami, Yuui Nakano, Soumya Kundu, Shinji Wada, Takumi Ikenoue, Masao Miyake, Tetsuji Hirato, and Maksud I. Saidaminov, Scalable fabrication of metal halide perovskites for direct X-ray flat-panel detectors: A perspective, *Chem. Mater.* **34**, 5323 (2022).
 - [8] Ling-Zhi Lei, Zhi-Feng Shi, Ying Li, Zhuang-Zhuang Ma, Fei Zhang, Ting-Ting Xu, Yong-Tao Tian, Di Wu, Xin-Jian Li, and Guo-Tong Du, High-efficiency and air-stable photodetectors based on lead-free double perovskite $\text{Cs}_2\text{AgBiBr}_6$ thin films, *J. Mater. Chem. C* **6**, 7982 (2018).
 - [9] Raisa-Ioana Biega, Yinan Chen, Marina R. Filip, and Linn Leppert, Chemical mapping of excitons in halide double perovskites, *ArXiv:2306.11352* (2023).

- [10] Debasmita Pariari, Sakshi Mehta, Sayak Mandal, Arup Mahata, Titas Pramanik, Sujit Kamilya, Arya Vidhan, Tayur N. Guru Row, Pralay K. Santra, Shaibal K. Sarkar, *et al.*, Realizing the lowest bandgap and exciton binding energy in a two-dimensional lead halide system, *J. Am. Chem. Soc.* **145**, 15896 (2023).
- [11] Brenda Vargas, Germán Rodríguez-López, and Diego Solis-Ibarra, The emergence of halide layered double perovskites, *ACS Energy Lett.* **5**, 3591 (2020).
- [12] Eric T. McClure, Molly R. Ball, Wolfgang Windl, and Patrick M. Woodward, $\text{Cs}_2\text{AgBiX}_6$ ($X = \text{Cl}, \text{Br}, \text{I}$): new visible light absorbing, lead-free halide perovskite semiconductors, *Chem. Mater.* **28**, 1348 (2016).
- [13] Zhenyang Liu, Hanjun Yang, Junyu Wang, Yucheng Yuan, Katie Hills-Kimball, Tong Cai, Ping Wang, Aiwei Tang, and Ou Chen, Synthesis of lead-free $\text{Cs}_2\text{AgBiX}_6$ ($X = \text{Cl}, \text{Br}, \text{I}$) double perovskite nanoplatelets and their application in CO_2 photocatalytic reduction, *Nano Lett.* **21**, 1620 (2021).
- [14] Wan Deng, Zun-Yi Deng, Jiawei He, Mingzi Wang, Zi-Xuan Chen, Su-Huai Wei, and Hong-Jian Feng, Synthesis of $\text{Cs}_2\text{AgSbCl}_6$ and improved optoelectronic properties of $\text{Cs}_2\text{AgSbBr}_6/\text{TiO}_2$ heterostructure driven by the interface effect for lead-free double perovskites solar cells, *Appl. Phys. Lett.* **111**, 151602 (2017).
- [15] Fengxia Wei, Zeyu Deng, Shijing Sun, Noor Titan Putri Hartono, Hwee Leng Seng, Tonio Buonassisi, Paul D. Bristow, and Anthony K. Cheetham, Enhanced visible light absorption for lead-free double perovskite $\text{Cs}_2\text{AgSbBr}_6$, *Chem. Commun.* **55**, 3721 (2019).
- [16] Jiajun Luo, Shunran Li, Haodi Wu, Ying Zhou, Yang Li, Jing Liu, Jinghui Li, Kanghua Li, Fei Yi, Guangda Niu, *et al.*, $\text{Cs}_2\text{AgInCl}_6$ double perovskite single crystals: parity forbidden transitions and their application for sensitive and fast UV photodetectors, *ACS Photonics* **5**, 398 (2018).
- [17] Federico Locardi, Matilde Cirignano, Dmitry Baranov, Zhiya Dang, Mirko Prato, Filippo Drago, Maurizio Ferretti, Valerio Pinchetti, Marco Fanciulli, Sergio Brovelli, *et al.*, Colloidal synthesis of double perovskite $\text{Cs}_2\text{AgInCl}_6$ and Mn-doped $\text{Cs}_2\text{AgInCl}_6$ nanocrystals, *J. Am. Chem. Soc.* **140**, 12989 (2018).
- [18] Zewen Xiao, Ke-Zhao Du, Weiwei Meng, Jianbo Wang, David B. Mitzi, and Yanfa Yan, Intrinsic instability of $\text{Cs}_2\text{In}(i)\text{m}(iii)\text{x}6$ ($M = \text{Bi}, \text{Sb}; X = \text{Halogen}$) double perovskites: A combined density functional theory and experimental study, *J. Am. Chem. Soc.* **139**, 6054 (2017).
- [19] Xin-Gang Zhao, Ji-Hui Yang, Yuhao Fu, Dongwen Yang, Qiaoling Xu, Liping Yu, Su-Huai Wei, and Lijun Zhang, Design of lead-free inorganic halide perovskites for solar cells via cation-transmutation, *J. Am. Chem. Soc.* **139**, 2630 (2017).
- [20] Adam H. Slavney, Te Hu, Aaron M. Lindenberg, and Hemamala I. Karunadasa, A bismuth-halide double perovskite with long carrier recombination lifetime for photovoltaic applications, *J. Am. Chem. Soc.* **138**, 2138 (2016).
- [21] Raisa-Ioana Biega, Marina R. Filip, Linn Leppert, and Jeffrey B. Neaton, Chemically localized resonant excitons in silver-pnictogen halide double perovskites, *J. Phys. Chem. Lett.* **12**, 2057 (2021).
- [22] Adam D. Wright, Leonardo R. V. Buizza, Kimberley J. Savill, Giulia Longo, Henry J. Snaith, Michael B. Johnston, and Laura M. Herz, Ultrafast excited-state localization in $\text{Cs}_2\text{AgBiBr}_6$ double perovskite, *J. Phys. Chem. Lett.* **12**, 3352 (2021).
- [23] Peigeng Han, Cheng Luo, Wei Zhou, Jie Hou, Cheng Li, Daoyuan Zheng, and Keli Han, Band-gap engineering of lead-free iron-based halide double-perovskite single crystals and nanocrystals by an alloying or doping strategy, *J. Phys. Chem. C* **125**, 11743 (2021).
- [24] Hang Yin, Yeming Xian, Yongli Zhang, Weijian Chen, Xiaoming Wen, Naveed Ur Rahman, Yi Long, Baohua Jia, Jiandong Fan, and Wenzhe Li, An emerging lead-free double-perovskite $\text{Cs}_2\text{AgFeCl}_6$: In single crystal, *Adv. Funct. Mater.* **30**, 2002225 (2020).
- [25] Yuqiao Zhou, Abdelrahman M. Askar, Jan-Hendrik Pöhls, Abishek K. Iyer, Anton O. Oliynyk, Karthik Shankar, and Arthur Mar, Hexagonal double perovskite $\text{Cs}_2\text{AgCrCl}_6$, *Z. für Anorg. Allg. Chem.* **645**, 323 (2019).
- [26] Wenzhe Li, Naveed Ur Rahman, Yeming Xian, Hang Yin, Yunkai Bao, Yi Long, Songyang Yuan, Yangyi Zhang, Yaxuan Yuan, and Jiandong Fan, Regulation of the order-disorder phase transition in a $\text{Cs}_2\text{NaFeCl}_6$ double perovskite towards reversible thermochromic application, *J. Semicond.* **42**, 072202 (2021).
- [27] Xiangrong Cao, Lei Kang, Shaoxing Guo, Minggang Zhang, Zheshuai Lin, and Jianhua Gao, $\text{Cs}_2\text{NaVCl}_6$: A Pb-free halide double perovskite with strong visible and near-infrared light absorption, *ACS Appl. Mater. Interfaces* **11**, 38648 (2019).
- [28] Christopher J. Bartel, Jacob M. Clary, Christopher Sutton, Derek Vigil-Fowler, Bryan R. Goldsmith, Aaron M. Holder, and Charles B. Musgrave, Inorganic halide double perovskites with optoelectronic properties modulated by sublattice mixing, *J. Am. Chem. Soc.* **142**, 5135 (2020).
- [29] Suhail A. Dar, Basharat Want, and Shakeel Ahmad Khandy, Computer based predictions of structural stability and systematic study of magneto-electronic and optical properties of lead free halide double perovskites: Cs_2KxCl_6 : $X = \text{Co}$ and Ni , *J. Magn. Magn. Mater.* **545**, 168603 (2022).
- [30] Bo Cai, Xi Chen, Meiqiu Xie, Shengli Zhang, Xuhai Liu, Jinlong Yang, Wenhan Zhou, Shiying Guo, and Haibo Zeng, A class of Pb-free double perovskite halide semiconductors with intrinsic ferromagnetism, large spin splitting and high Curie temperature, *Mater. Horiz.* **5**, 961 (2018).
- [31] Manish Kumar, Brijmohan Prajapati, Abhishek Raj, Avneesh Anshul, Prakash Chandra Sati, Mohit Sahni, and Arvind Kumar, Progresses and challenges in the structural and magnetic properties of double perovskite $\text{La}_2\text{NiMnO}_6$ with their applications in solar energy, *Mater. Today: Proc.* **49**, 3088 (2022).
- [32] David S. Walch, Yeseul Yun, Niranjan Ramakrishnegowda, Lutz Mühlenein, Andriy Lotnyk, Cameliu Hincinschi, and Akash Bhatnagar, Resistive switching in ferroelectric $\text{Bi}_2\text{FeCrO}_6$ thin films and impact on the photovoltaic effect, *Adv. Electron. Mater.* **8**, 2200276 (2022).
- [33] Qingxia Fu, Xianglan Tang, Bin Huang, Ting Hu, Licheng Tan, Lie Chen, and Yiwang Chen, Recent progress on the long-term stability of perovskite solar cells, *Adv. Sci.* **5**, 1700387 (2018).

- [34] Jurgen Hafner and Georg Kresse, In *Properties of Complex Inorganic Solids* (Springer US, Boston, MA, 1997), p. 69.
- [35] Jürgen Hafner, Materials simulations using VASP—a quantum perspective to materials science, *Comput. Phys. Commun.* **177**, 6 (2007).
- [36] Peter E. Blöchl, Projector augmented-wave method, *Phys. Rev. B* **50**, 17953 (1994).
- [37] John P. Perdew and Wang Yue, Accurate and simple density functional for the electronic exchange energy: Generalized gradient approximation, *Phys. Rev. B* **33**, 8800 (1986).
- [38] John P. Perdew, K. Burke, and M. Ernzerhof, Perdew, Burke, and Ernzerhof reply, *Phys. Rev. Lett.* **80**, 891 (1998).
- [39] Georg Kresse and Daniel Joubert, From ultrasoft pseudopotentials to the projector augmented-wave method, *Phys. Rev. B* **59**, 1758 (1999).
- [40] Richard T. Scalettar, An introduction to the Hubbard Hamiltonian, *Quantum Mater.: Exp. Theory* **6**, 1 (2016).
- [41] Matteo Cococcioni and Stefano De Gironcoli, Linear response approach to the calculation of the effective interaction parameters in the LDA + U method, *Phys. Rev. B* **71**, 035105 (2005).
- [42] See Supplemental Material at <http://link.aps.org/supplemental/10.1103/PhysRevApplied.21.014063> for the method of self-consistent calculation of Coloumb interaction parameters for the present series (for values, see Table S1). Calculation of Goldschmidt's tolerance factor along with the values (Table S2), the formation energies (Table S3) of all compounds in the 3d transition-metal double-perovskite series stable in the respective magnetic states, detailed analysis of chemical stability along with the magnetic ordering and space group of secondary phases (Table S4) and phases diagrams (Fig. S2), pressure variation of chemical stability of $\text{Cs}_2\text{AgFeCl}_6$ and $\text{Cs}_2\text{AgCrCl}_6$ (Fig. S3), dynamic stability study (Fig. S4), detailed study of the electronic structure of the rest of the members of the series along with the band gap and magnetic moments (Table S5) and band diagrams along with the density of states (Figs. S5–S8), and temperature dependence of carrier mobilities of $\text{Cs}_2\text{AgBiBr}_6$, $\text{Cs}_2\text{AgFeCl}_6$, and $\text{Cs}_2\text{AgCrCl}_6$ at a carrier concentration of 10^{10} cm^{-3} (Fig. S9).
- [43] Sergei L. Dudarev, Gianluigi A. Botton, Sergey Y. Savrasov, C. J. Humphreys, and Adrian P. Sutton, Electron-energy-loss spectra and the structural stability of nickel oxide: An LSDA+U study, *Phys. Rev. B* **57**, 1505 (1998).
- [44] Maituo Yu, Shuyang Yang, Chunzhi Wu, and Noa Marom, Machine learning the Hubbard U parameter in DFT+U using Bayesian optimization, *npj Comput. Mater.* **6**, 180 (2020).
- [45] Yingying Wang, Hanlin Huang, Zhenzhen Zhang, Cong Wang, Yuying Yang, Qi Li, and Dongsheng Xu, Lead-free perovskite $\text{Cs}_2\text{AgBiBr}_6@\text{g-C}_3\text{N}_4$ Z-scheme system for improving CH_4 production in photocatalytic CO_2 reduction, *Appl. Catal. B: Environ.* **282**, 119570 (2021).
- [46] Ahmed Mahmoud Idris, Taifeng Liu, Jafar Hussain Shah, Hongxian Han, and Can Li, $\text{Sr}_2\text{CoTaO}_6$ double perovskite oxide as a novel visible-light-absorbing bifunctional photocatalyst for photocatalytic oxygen and hydrogen evolution reactions, *ACS Sustain. Chem. Eng.* **8**, 14190 (2020).
- [47] Akio Ikesue and Yan Lin Aung, in *Processing of Ceramics: Breakthroughs in Optical Materials* (John Wiley & Sons, Hoboken, NJ, USA, 2021), p. 143.
- [48] Hyun Cheol Koo, Seong Been Kim, Hansung Kim, Tae-Eon Park, Jun Woo Choi, Kyoung-Whan Kim, Gyungchoon Go, Jung Hyun Oh, Dong-Kyu Lee, Eun-Sang Park, *et al.*, Rashba effect in functional spintronic devices, *Adv. Mater.* **32**, 2002117 (2020).
- [49] Luiz Gustavo Davanse da Silveira, Paolo Barone, and Silvia Picozzi, Rashba-Dresselhaus spin-splitting in the bulk ferroelectric oxide BiAlO_3 , *Phys. Rev. B* **93**, 245159 (2016).
- [50] Chang Ming Fang, G. A. De Wijs, and R. A. De Groot, Spin-polarization in half-metals, *J. Appl. Phys.* **91**, 8340 (2002).
- [51] G. A. De Wijs and R. A. De Groot, Towards 100% spin-polarized charge-injection: The half-metallic NiMnSb/CdS interface, *Phys. Rev. B* **64**, 020402 (2001).
- [52] Liping Yu and Alex Zunger, Identification of potential photovoltaic absorbers based on first-principles spectroscopic screening of materials, *Phys. Rev. Lett.* **108**, 068701 (2012).
- [53] V. M. Goldschmidt, Crystal structure and chemical constitution, *Trans. Faraday Soc.* **25**, 253 (1929).
- [54] Christopher J. Bartel, Christopher Sutton, Bryan R. Goldsmith, Runhai Ouyang, Charles B. Musgrave, Luca M. Ghiringhelli, and Matthias Scheffler, New tolerance factor to predict the stability of perovskite oxides and halides, *Sci. Adv.* **5**, eaav0693 (2019).
- [55] Wei Li, Zheming Wang, Felix Deschler, Song Gao, Richard H. Friend, and Anthony K. Cheetham, Chemically diverse and multifunctional hybrid organic–inorganic perovskites, *Nat. Rev. Mater.* **2**, 1 (2017).
- [56] Lingyuan Gao, Lena Yadgarov, Rituraj Sharma, Roman Korobko, Kyle M. McCall, Douglas H. Fabini, Constantinos C. Stoumpos, Mercouri G. Kanatzidis, Andrew M. Rappe, and Omer Yaffe, Metal cation s lone-pairs increase octahedral tilting instabilities in halide perovskites, *Mater. Adv.* **2**, 4610 (2021).
- [57] Ruo Xi Yang, Jonathan M. Skelton, Estelina L. Da Silva, Jarvis M. Frost, and Aron Walsh, Assessment of dynamic structural instabilities across 24 cubic inorganic halide perovskites, *J. Chem. Phys.* **152**, 024703 (2020).
- [58] W. Travis, E. N. K. Glover, H. Bronstein, D. O. Scanlon, and R. G. Palgrave, On the application of the tolerance factor to inorganic and hybrid halide perovskites: A revised system, *Chem. Sci.* **7**, 4548 (2016).
- [59] Peter Köhl, Ulrich Müller, and Dirk Reinen, $\text{Ba}_2\text{NiTeO}_6$ – eine neue Verbindung in der Reihe der hexagonalen Perowskite, *Z. Anorg. Allg. Chem.* **392**, 124 (1972).
- [60] Pratap Vishnoi, Ram Seshadri, and Anthony K. Cheetham, Why are double perovskite iodides so rare? *J. Phys. Chem. C* **125**, 11756 (2021).
- [61] Jie Xue, Ziyu Wang, Andrew Comstock, Zhiyu Wang, Herman H. Y. Sung, Ian D. Williams, Dali Sun, Junwei Liu, and Haipeng Lu, Chemical control of magnetic ordering in hybrid Fe–Cl layered double perovskites, *Chem. Mater.* **34**, 2813 (2022).
- [62] Michael C. Brennan, Sergiu Draguta, Prashant V. Kamat, and Masaru Kuno, Light-induced anion phase segregation in mixed halide perovskites, *ACS Energy Lett.* **3**, 204 (2017).

- [63] Sebastian Caicedo-Davila, Hannah Funk, Robert Lovrinic, Christian Müller, Michael Sendner, Oana Cojocaru-Miredin, Frederike Lehmann, Rene Gunder, Alexandra Franz, Sergej Levcenco, *et al.*, Spatial phase distributions in solution-based and evaporated Cs–Pb–Br thin films, *J. Phys. Chem. C* **123**, 17666 (2019).
- [64] Zhuo-Liang Yu, Yu-Qing Zhao, Qiang Wan, Biao Liu, Jun-Liang Yang, and Meng-Qiu Cai, Exploring the coexistence mechanism of CsPb_2Br_5 and CsPbBr_3 based on the competitive phase diagram, *J. Phys. Chem. C* **124**, 23052 (2020).
- [65] Nathan R. Wolf, Adam Jaffe, Adam H. Slavney, Wendy L. Mao, Linn Leppert, and Hemamala I. Karunadasa, Tuning defects in a halide double perovskite with pressure, *J. Am. Chem. Soc.* **144**, 20763 (2022).
- [66] Julian Gebhardt and Christian Elsässer, The electronic structure of $\text{Cs}_2\text{AgBiBr}_6$ at room temperature, *Phys. Status Solidi (b)* **259**, 2200124 (2022).
- [67] Johan Klarbring, Olle Hellman, Igor A. Abrikosov, and Sergei I. Simak, Anharmonicity and ultralow thermal conductivity in lead-free halide double perovskites, *Phys. Rev. Lett.* **125**, 045701 (2020).
- [68] Jack Yang and Sean Li, An atlas of room-temperature stability and vibrational anharmonicity of cubic perovskites, *Mater. Horiz.* **9**, 1896 (2022).
- [69] Ling-yi Huang and Walter R. L. Lambrecht, Electronic band structure trends of perovskite halides: Beyond Pb and Sn to Ge and Si, *Phys. Rev. B* **93**, 195211 (2016).
- [70] Alex M. Ganose, Junsoo Park, Alireza Faghaninia, Rachel Woods-Robinson, Kristin A. Persson, and Anubhav Jain, Efficient calculation of carrier scattering rates from first principles, *Nat. Commun.* **12**, 2222 (2021).
- [71] R. Del Sole and Raffaello Girlanda, Optical properties of semiconductors within the independent-quasiparticle approximation, *Phys. Rev. B* **48**, 11789 (1993).
- [72] Valerio Lucarini, Jarkko J. Saarinen, Kai-Erik Peiponen, and Erik M. Vartiainen, *Kramers-Kronig Relations in Optical Materials Research* (Springer Science & Business Media, New York, 2005), Vol. 110.
- [73] Yang Zhang, Tobias Holder, Hiroaki Ishizuka, Fernando de Juan, Naoto Nagaosa, Claudia Felser, and Binghai Yan, Switchable magnetic bulk photovoltaic effect in the two-dimensional magnet CrI_3 , *Nat. Commun.* **10**, 3783 (2019).